The Thesis committee for Austin Lee Blackmon Certifies that this is the approved version of the following thesis.

Electron Temperature Gradient Mode Streamers and the End of the Tokamak Pedestal

APPROVED BY

SUPERVISING COMMITTEE:

Richard Hazeltine, Supervisor

Swadesh Mahajan

Electron Temperature Gradient Mode Streamers and the End of the Tokamak Pedestal

by

Austin Lee Blackmon

THESIS

Presented to the Faculty of the Graduate School of

The University of Texas at Austin

in Partial Fulfillment

of the Requirements

for the Degree of

MASTER OF ARTS

THE UNIVERSITY OF TEXAS AT AUSTIN

December 2019

Dedicated to

Jackie C. Smith (1937-2018)

and

Franki W. Aymond (1988-2019)

Acknowledgments

I would like to express gratitude to have worked with:

- Dr. Richard Hazeltine
- Dr. Mike Kotschenreuther
- Dr. David Hatch
- Dr. Craig Michoski

and for their guidance and support through my research.
I would also like to thank family and friends for their continued support.

Electron Temperature Gradient Mode Streamers and the End of the Tokamak Pedestal

Austin Lee Blackmon, M.A.
The University of Texas at Austin, 2019

Supervisor: Richard Hazeltine

Fusion experiments still show discrepancies in heat flux from expected results calculated from theory and computation; calculations come up short. As needed, work continues in solving the source of these discrepancies. This thesis seeks to provide part of the answer via electron-temperature-gradient (ETG) fluctuations in the pedestal region of tokamaks, investigated with the Gyrokinetic Electromagnetic Numerical Experiment (GENE). While ETG turbulence is sometimes ignored, as it is very small scale, there may be mechanisms that make it a viable explanation of these discrepancies. In this work, we find a non-negligible heat transport from ETG turbulence in the presence of streamers. Additionally, we find a relation between flux, streamers, and velocity shear. Further analysis is required to confirm these findings, but as it stands, this thesis lays the groundwork.

Table of Contents

List of Tables

List of Figures

Chapter 1

Introduction

The root of magnetically-confined fusion problems is in the name, *confinement*. Confinement defines the ability to contain and control the plasma, which very basically can be defined by the Lawson criterion, $n\tau_E \geq 5 \times 10^{14}$ s/cm^3, where n is the density and τ_E is the energy confinement time. The value 5×10^{14} s/cm^3 is specifically for deuterium-tritium plasmas. The confinement time can be affected by a wide variety of phenomena, but this thesis will focus on turbulent transport, specifically transport caused by the electron-temperature-gradient (ETG) mode. Transport refers to the movement of energy, particles, and/or momentum across a flux surface within or at the edge of a plasma, and turbulent transport is such flux caused by turbulence in the plasma.

Transport has been extensively studied, but we are still left with discrepancies between experimental data and theoretical and computational calculations of transport values. Thus, there still exist underlying phenomena that have not been found or applied to the problem. Within the fusion community, many people are working to solve this discrepancy. One key area of study has been, and still is, drift waves. Drift waves are a mechanism of

turbulent transport that cause perturbations in the plasma which can lead to rapidly-growing instabilities. These instabilities shift the plasma out of equilibrium, causing unwanted transport out of the plasma. Drift waves have helped account for much of the lost transport, thus, the control of drift waves is a key for improving confinement time. In this thesis, we look at one type of drift wave, the aforementioned ETG mode.

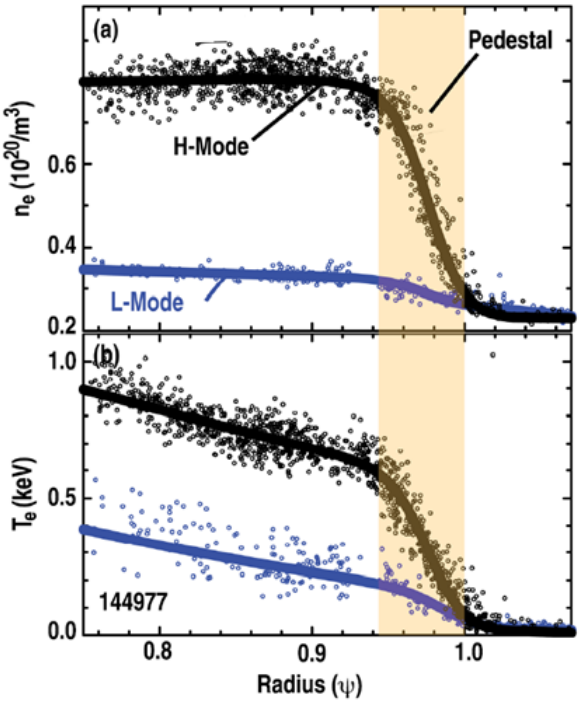

Figure 1.1: Shown is the last $\sim$ 25% of the temperature and density profiles, the region known as the pedestal, for JET shot 78697. At $r \approx 0.95$, the pedestal ends and at $r \approx 0.98$, we see the steepest gradient. Figure from A. W. Leaonard [15].

Another important source of confinement time improvement comes from the H-mode. The H-mode, or high-confinement mode, is an operating state of tokamaks that is defined by steep edge-temperature and -density profiles, a region referred to as the pedestal, as shown in Figure 1.1. As stated by W. M. Stacey, the H-mode comes about when the nonradiative power across the last closed flux surface (LCFS) exceeds,

$$P > (2.84/A_i)\bar{n}_{20}^{0.58}B^{0.82}Ra^{0.81} \tag{1.1}$$

where A_i is the ion mass (in amu), $\bar{n}_{20}$ is the line-average electron density (in 10^{20} m^{-3}), B is the toroidal magnetic field (in tesla), R is the major radius (in m), and a is the minor radius (in m) [20]. Prior to the discovery of the H-mode, tokamaks operated in what is referred to as the L-mode, low-confinement mode, also pictured in Figure 1.1. In the H-mode, further inward from the pedestal, the profiles grow linearly, as seen in L-modes. From this, we see that the height of the pedestal helps dictate core temperature and density, i.e., confinement, thus motivating investigation into how to control pedestal conditions to extend the height of the pedestal.

The pedestal region is typically the last few percent of the plasma radius, characterized by the rapidly growing temperature and density, as mentioned previously. The pedestal is a unique region within a tokamak, with some extreme conditions, including strong velocity shear. Tokamak regions with such conditions are called transport barriers, named such that the physical conditions within the regions inhibit transport. This thesis seeks to investigate a number of characteristics of ETG modes within the pedestal.

Through gyrokinetic simulations using the Gyrokinetic Electromagnetic Numerical Experiment (GENE), we investigate ETG driven turbulence within the pedestal region. A number of initial benchmarks and other linear simulations are run before working with data from Joint European Torus (JET) shot 78697. Beyond the benchmarks, we seek to confirm the linear consequences of electromagnetic (EM) effects and kinetic, often referred to non-adiabatic, ions within GENE for ETG pedestal simulations. At base, GENE uses electrostatic (ES) effects in simulations, while it also allows for the inclusion of electromagnetic effects. Including EM effects increases computation time, thus, if possible, it is helpful to use only ES effects to reduce computation time. Additionally, GENE allows users to specify the species that are used in the simulations. For example, one could run a simulation with electrons and ions, where GENE will evolve the profiles of all species through the simulation. However, the inclusion of multiple species also increases the computation time. A single species simulation in GENE, here we use only electrons, will treat the ion profile as a background profile that does not evolve with time, which we refer to as adiabatic ions. The inclusion of ions as a species is thus treating the ions as *kinetic* ions. It is important to reduce computation time where possible, thus motivating investigation into these effects. We find that in linear ETG pedestal simulations, the inclusion of EM effects and non-adiabatic ions does not affect growth rates, thus signifying that these effects can be left out in our nonlinear simulations.

We begin analysis of JET shot 78697 with linear runs to check growth rates at four separate radii. These runs give expected results – low growth rates at the pedestal top where temperature gradient is shallow and high growth rates where the temperature gradient is steep. From there a series of nonlinear simulations bring out unexpected results. We see non-negligible heat flux for ETG scale instabilities in the pedestal region, including at the top of the pedestal where there is a much shallower temperature gradient than in the middle of the pedestal. Because the predominant driver of this instability is the electron-temperature gradient, a currently unknown mechanism is causing this unexpectedly high heat flux at the pedestal top for ETG instabilities. One possibility lies in streamer formation at the pedestal top, which is observed in our results. Streamers are elongated radial structures that lead to cross-field transport and thus allow for increased heat flux out of the plasma, lowering confinement. We then check the effect of velocity shear on streamer formation and heat flux, finding that increased velocity shear results in smaller streamers and lower heat flux.

While these results provide evidence that ETG turbulence can produce non-negligible heat flux and is suppressed by velocity shear, analysis is incomplete. Verifying results with the inclusion of EM effects and kinetic ions in *nonlinear* simulations in GENE will help confirm the findings of our linear analysis. Additionally, further simulations using other shots must be undertaken. Strong candidates include shots from DIIID, seeking to confirm the findings do not depend on the device used, as well as additional shots

from JET, from other carbon wall and ITER-like wall shots. Additionally, studies beyond the outboard midplane will be necessary to explain what is happening throughout the tokamak.

Chapter 2

Background

2.1 Transport

In short, transport in a plasma is the flux of particles, heat, and/or momentum across a flux surface. Transport is incredibly important, as it tells you what, and how much of it, is moving through or leaving the plasma. If transport were small and completely controlled, magnetic fusion would have been solved decades ago. Unfortunately, this is not so.

The first formulation of transport, classical transport, was a simple model describing diffusive transport via Coulomb collisions. After that, neoclassical theory also brought in geometric effects of tokamaks, providing a more accurate description of transport. However, calculations via classical and neoclassical theory showed discrepancies from experimental measurements. The missing pieces were referred to as anomalous transport.

2.2 Fluctuations and transport

As anomalous transport was investigated, a strong correlation between fluctuations of plasma parameters, e.g., temperature, density, potential, etc, and transport was found by experiment [18]. It was later found that these

fluctuations induced a wide variety of microturbulences that account for some of the missing transport. While it is generally agreed upon that this microturbulence-induced transport is the missing piece of the puzzle, there are areas where turbulent transport still falls short, one being within the pedestal.

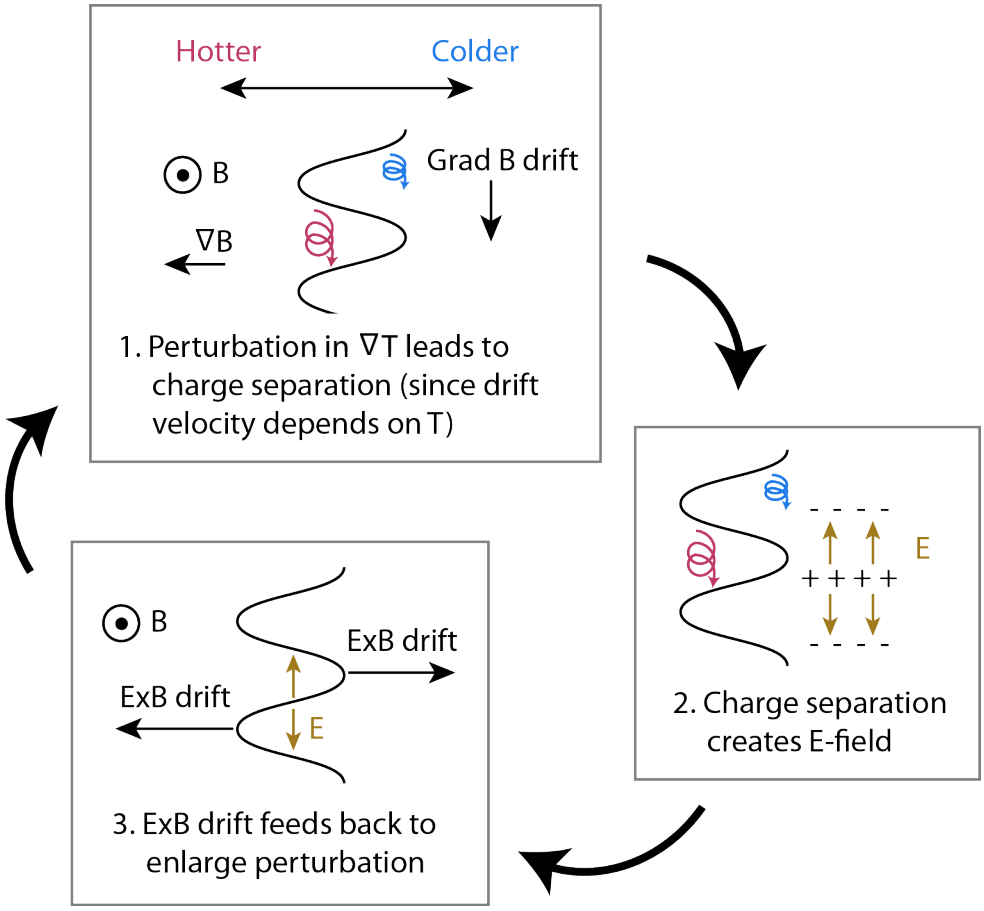

Figure 2.1: Diagram of ion-temperature-gradient instability. A perturbation in the temperature gradient causes a charge separation, creating an electric field. The electric field then causes an E×B drift, furthering the instability. Figure from FusionWiki [3].

2.3 Drift waves

Drift waves, first described using fluid models, are waves with perturbation frequencies of order $\omega \approx kv_d$, where v_d is the drift velocity. The drift velocity accounts for any and all drifts that are acting on a particle, including the ∇B drift and the $E \times B$ drift.

2.4 Electron-temperature-gradient turbulence

Electron-temperature-gradient (ETG) turbulence is driven, as the name suggests, by gradients in the electron temperature profile. Perturbations in the temperature gradient cause a charge separation, as the drift velocity depends on temperature. This charge separation induces an electric field, causing $E \times B$ drifts in opposing relative directions that leads to a further perturbation in temperature gradient. If these perturbations are not controlled, a runaway instability can occur. A similar mode is the ion-temperature-gradient, shown in Figure 2.1.

2.5 Gyrokinetics

Gyrokinetics is an approximation of kinetic plasma motion. In gyrokinetics, particle positions are not tracked, rather their guiding center is tracked. Given gyrokinetic ordering, we can approximate a particle's orbit around a magnetic field line as the particle's position, given that the gryroradius is much smaller than equilibrium scale lengths and gyrofrequency is much

smaller than equilibrium time scales. Additionally, parallel wave numbers are much smaller than perpendicular wave numbers. We also state that perturbed quantities are much smaller scale than equilibrium quantities. Gyrokinetic ordering can thus be written out by,

$$\frac{\rho_\sigma}{a} \sim \frac{\omega}{\Omega_\sigma} \sim \frac{|\delta B|}{|B|} \sim \frac{|\delta E|}{|E|} \sim \frac{k_\parallel}{k_\perp} \sim \frac{\delta f_\sigma}{f_\sigma} \leq \epsilon. \tag{2.1}$$

The gyrokinetic Vlasov equation is then given by,

$$\frac{\partial f_\sigma}{\partial t} + \dot{X} \cdot \nabla f_\sigma + \dot{\mu} \frac{\partial f_\sigma}{\partial \mu} + \dot{v}_\parallel \frac{\partial f_\sigma}{\partial v_\parallel} = 0, \tag{2.2}$$

for species σ, with the gyrocenter position given by X.

Gyrokinetics plays a very important role in the computational study of plasma turbulence. G. Hammett estimates that from a move to gyrokinetic equations from standard Vlasov systems, computation speed has increased by a factor of 10^{11} [5]. Gyrokinetics also works very well for simulation of microturbulence, including ETG, thus a gyrokinetic code is chosen for this work. While there are many promising gyrokinetic codes to choose from, we choose to work with the Gyrokinetic Electromagnetic Numerical Experiment (GENE), as GENE is specifically designed to model plasma microturbulence [7].

2.6 Gyrokinetic Electromagnetic Numerical Experiment

The Gyrokinetic Electromagnetic Numerical Experiment is a nonlinear plasma microturbulence differential-equation solver written in Fortran,

specifically designed for computing gyroradius-scale fluctuations and transport. For geometry, GENE takes a flux-tube approach, as is common for microturbulence problems. And, as is common for gyrokinetic problems, GENE uses a reduced five-dimensional phase space, three spatial dimensions, one momentum dimension, and one magnetic moment dimension, in addition to the necessary temporal dimension.

Both global and local simulations can be run in GENE. Global simulations treat the entire tokamak as the simulation domain, whereas local simulations are smaller domains that follow a magnetic field line given a flux-tube model, shown later. In this thesis, we use only local simulations, thus will ignore any description of global simulations. Local simulations use a radially dependent Krook-like energy source and sink model [5].

2.6.1 Paramaters

To set up a simulation, GENE uses an input parameters file that allows a great deal of customization. This section will cover the parameters used, with a brief description of each. The parameters are separated by sections called namelists, including parallelization, geometry, and species.

`paralellilization` namelist contains parameters controlling how to parallelize the simulation. Number of processors is chosen for each dimension, species, and for the simulation as a whole.

`box` namelist contains parameters controlling the size and location of the simulation space, as well as the number of species. For box size, one must take

care as the y-dimension is treated differently than all other dimensions. `nx0`, `nz0`, `nv0`, and `nw0` give the grid size for the x, z, velocity, and magnetic moment dimensions, while `nky0` gives the number of Fourier modes in the y-dimension. The box width in the x-dimension is set with `lx`, and the flux surface radius is set with `x0`. The box height in the y-dimension is then set with `kymin`, the minimum k_y mode in the simulation, given in inverse gyroradii, corresponding to a size of $2\pi/$`kymin`.

`in_out` namelist contains parameters controlling file handling, such as output directory, reading and writing of checkpoints, and step size for various calculated quantities, for which output files are created. In this namelist, `iterdb_file` points to an .iterdb file, typically generated from experimental data.

`general` namelist contains many parameters controlling basic physical conditions such as plasma beta, `beta`, and the Debye length, `debye2`, as well as the collision frequency, `coll`, and collision operator, `collision_op`. Controls for max simulation time are also contained in this namelist.

`external_contr` namelist contains external controls enacted on the simulation, for this work, we only look at `ExBrate`, which controls the level of induced velocity shear.

`geometry` namelist contains parameters for the geometry of the system. Basic geometries, such as the s-alpha geometry used for a portion of this work, may be used or a geometry file produced via experiments can be loaded using

`geomfile` Also in this namelist, the safety factor is given by `q0` and magnetic shear is given by `shat`.

`species` namelist contains information for all of the species used in the simulation. Temperature and density gradients, mass, temperature, density, and charge are required for all species. The temperature gradient is given by `omt`, and the density gradient is given by `omn`, which will be referred to later as omt and omn.

Additionally, for linear simulations, GENE allows for scans to be performed. Scans allow one to set up a series of simulations scanning over a specific parameter, such as `kymin` or `omt`. We will refer to these series of simulations later as k_y and omt or ω_T scans.

2.6.2 Differential equations

The nonlinear differential equation solved by GENE is given by,

$$\frac{\partial g}{\partial t} = Z + \mathcal{L}[g] + \mathcal{N}[g], \tag{2.3}$$

where g is the distribution function of all species, Z is a constant term containing effects of curvature and gradients, $\mathcal{L}$ is the linear operator, and $\mathcal{N}$ is the nonlinear operator. The constant term and operators are given by,

$$Z = \frac{T_{0j}\left(2v_{\parallel}^2 + \mu B_0\right)}{q_j B_0} K_x \left(\omega_n + \left(v_{\parallel}^2 + \mu B_0 - \frac{3}{2}\right)\omega_{Tj}\right)\delta_{k_x,0}\delta_{k_y,0}F_{0j},$$

$$\mathcal{L}[g] = -\left(\omega_n + \left(v_\parallel^2 + \mu B_0 - \frac{3}{2}\right)\omega_{Tj}\right) F_{0j} i k_y \chi + \frac{\beta T_{0j}}{q_j B_0^2} v_\parallel^2 \omega_p \Gamma_{jy} - \frac{v_{Tj}}{J B_0} v_\parallel \Gamma_{jz}$$
$$- \frac{T_{0j}\left(2v_\parallel^2 + \mu B_0\right)}{q_j B_0}\left(K_y \Gamma_{jy} + K_x \Gamma j x\right) + \frac{v_{Tj}}{2JB_0}\mu \partial_z B_0 \frac{\partial f_j}{\partial v_\parallel} + \langle C_j(f)\rangle\,,$$

$$\mathcal{N}[g] = \sum_{\vec{k}'_\perp} (k'_x k_y - k_x k'_y)\chi(\vec{k}'_\perp) g_j(\vec{k}_\perp - \vec{k}'_\perp).$$

These operators and their derivations are described in detail by Merz [17].

2.6.3 Geometry

To work with the flux-tube model mentioned previously, GENE uses magnetic-flux coordinates, which follow and bend around the magnetic field lines. The coordinate transformation is given by,

$$x = \frac{q_0}{r_0 B_0}\psi \tag{2.4}$$
$$y = \frac{r_0}{q_0}(q(\psi)\theta - \zeta) \tag{2.5}$$
$$z = \theta, \tag{2.6}$$

where x is a radial-like coordinate, y follows the flux surface perpendicular to x and the field line at the given x, and z follows the field line. This model works well for microturbulence, as microturbulence is flute-like, i.e., long parallel wavelengths and short perpendicular wavelengths.

The flux-tube model simulation space consists of a curved and sheared box around a central field line, denoted as x_0. The box dimensions consist of one parallel (to the magnetic-field axis) dimension, denoted as the z-axis, and

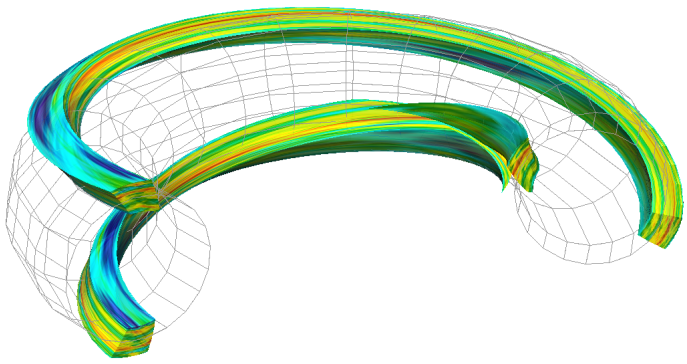

Figure 2.2: Example of a flux tube model, generated by the Gyro-kinetic Workshop (GKW) code [8]. The flux tube follows a magnetic field line around the tokamak.

two perpendicular dimensions, denoted as the x- and y-axes. The length of the box in the x- and y-dimensions must be larger than any structures that the simulation is probing, i.e., they must be longer than correlation lengths and mode lengths. The box length is set by defining `lx` and `kymin` in the GENE `parameters` file, as stated previously.

Chapter 3

Results

The simulations in this thesis were run on the Department of Energy (DoE) Edison supercomputer at the National Energy Research Scientific Computing Center (NERSC). Edison is a Cray XC30 with 2.57 petaflops peak performance on 134,064 compute cores, supplied by Intel Xeon E5-2695v2 processors. Edison has since been retired, replaced by the new Cray XC40 computer Cori [1].

Through simulations using GENE, we find an interesting relationship of streamer formation on heat-flux produced by ETG modes in the tokamak pedestal. However, before any original work is done, it is necessary to benchmark the installation of GENE by running a number of simulations based on well-analyzed systems and shots. We run a series of linear scans using a parameters from a well-known DIIID shot, 98669, generally referred to as the cyclone case, often used to benchmark code. A number of parameter changes are made to further verify the code installation. We then look, in the linear regime, for the dependence of non-adiabatic ions on our system. In GENE, adiabatic ions refer to using a constant background profile for the ions, whereas non-adiabatic ions refer to an ion profile that evolves in

time with the system. We also test for the effect of including electromagnetic physics on top of the base electrostatic physics. We also test these effects in the purely theoretical s-alpha geometry. We then move onto JET run 78697. The analysis of this run is the primary finding of this thesis.

The shot shows a non-negligible heat flux throughout the pedestal from ETG turbulence. As expected, the largest heat flux exists at the high-gradient region (center) of the pedestal. As ETG is a temperature-driven instability, it is expected that a small heat-flux exists at low-temperature gradients. However, we find that even at the low-gradient region (top) of the pedestal, still a significantly large heat-flux exists. This finding motivates the thinking that a large portion of ETG turbulence is brought on by nonlinear effects.

3.1 Preliminary simulations

A number of initial simulations are run to check the performance of our new installation of GENE on Edison. Initially, running linear simulations, we check an unaltered cyclone benchmarking case k_y scan for ITG modes, comparing it against a GS2 scan of the same k_y values [9]. Then we run a set of cyclone scans checking for known behavior in typical parameter regimes, also for ITG modes. We then run a temperature gradient scan for ETG modes, comparing adiabatic and kinetic ions for two values of T_i/T_e. Last, we run a set of k_y scans, varying the Debye length for values found in relevant devices, as well as another test of adiabatic vs kinetic ions for $\lambda_D = 0$.

We then move onto a variety of linear simulations using basic s-alpha

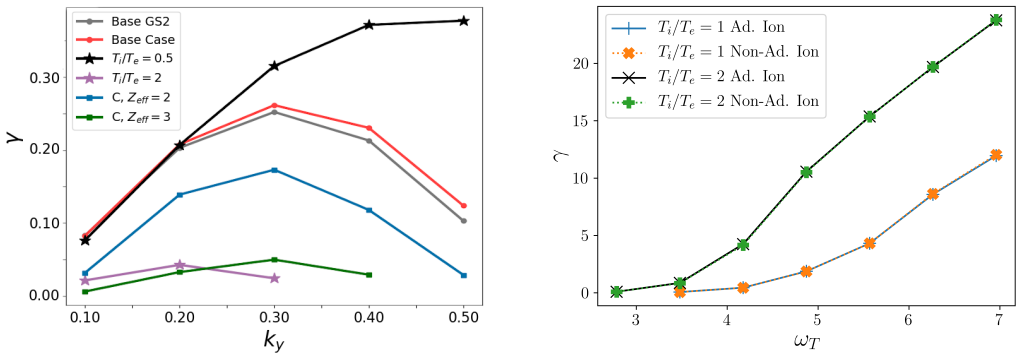

Figure 3.1: Left shows growth rate vs k_y for ITG cyclone base case scan, in red, against a GS2 scan of the cyclone base case [9], and a variety of runs with parameter changes. Parameters changed are T_i/T_e and Z_{eff}, derived by adding carbon impurities. Close comparison with the GS2 run verifies our GENE installation is comparable to prior accepted results. Right shows temperature gradient scans for cyclone base case with JET-like Debye length, over typical values for a JET pedestal.

geometry, verifying that adiabatic vs kinetic ions do not change results of growth rates significantly. We verify that including electromagnetic effects also does not significantly change growth rates.

3.1.1 Cyclone Benchmarking

The cyclone benchmarking case is loosely based on a DIIID discharge, a commonly used case to benchmark code. Here, we use the cyclone case to test our installation of GENE and to check for dependence of electromagnetic effects and kinetic ions on linear growth rates. The cyclone case can be simulated using a specific set of parameters with s-alpha geometry. The parameters we set, `shat=0.796`, `trpeps=0.18`, `omt=6.92`, `omn=2.22`, `beta=0`,

q0=1.4, adiabatic electrons, single ion species, with electron temperature equal to ion temperature. For all of the cyclone runs, we use 4 processors per run, using a box size of nx0=22, nky0=1, nz0=48, nv0=32, nw0=8. We then vary a number of parameters over many series of runs.

3.1.1.1 ITG mode comparison

We run the cyclone base case, as well as various parameter changes to further check that the code is working, shown in Figure 3.1. The unchanged case, in red, was initially compared against a set of runs from GS2, in gray, showing good agreement [9]. Increasing and decreasing T_i/T_e by a factor of two changes linear growth rates, decreasing γ for the former, and increasing γ for the latter, as expected from the linear growth rate model [20]. Additionally, we add carbon impurities by changing Z_{eff} by a factor of two and a factor of three. Again, we see expected changes, with impurities stabilizing the ITG mode, lowering the growth rates.

3.1.1.2 ETG mode with JET parameters

The next set of runs, also shown in Figure 3.1, are ETG temperature-gradient scans, using the Debye length found in JET. The temperature-gradient varies over values commonly found in a JET pedestal. Initially, we check for further destabilization of the ETG instability from increased T_i/T_e, opposite of what we see for ITG modes, which we confirm. We do an additional check for the effect of using kinetic ions, again finding no change from using adiabatic ions.

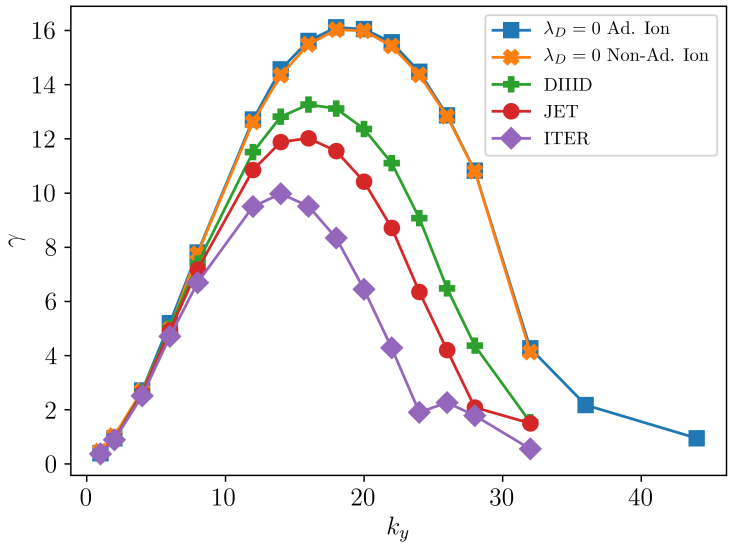

Figure 3.2: Shown are ETG cyclone scans, with Debye length set to 0 for adiabatic and non-adiabatic ions. Also included are cyclone ETG scans with Debye length set to typical values seen in DIIID, JET, and ITER, increasing relatively.

3.1.1.3 ETG mode for relevant devices

For our last set of cyclone runs, we scan over k_y, varying the Debye length for values found in DIIID, JET, and ITER (expected), as well as another test of adiabatic vs kinetic ions for $\lambda_D = 0$, shown in Figure 3.2. All scans run k_y from 2 up to 30-40.

3.1.2 S-alpha geometry

The base parameter setup for our initial s-alpha scan uses the same parallelization and box size as our cyclone runs. For collisions, we use

GENE's Landau collision operator. These runs are single species, using adiabatic ions. Density gradient is set to 0 and temperature gradient is set to 25. Electromagnetic effects are also turned off for this scan.

In addition to the initial scan, three more scans are run to test the effect of non-adiabatic ions and electromagnetic effects on the growth rate. The three additional scans run through adiabatic ions with electromagnetic effects on, non-adiabatic ions with only electrostatic effects, and non-adiabatic ions with electromagnetic effects on. Growth rates for each of these runs are shown in Figure 3.3.

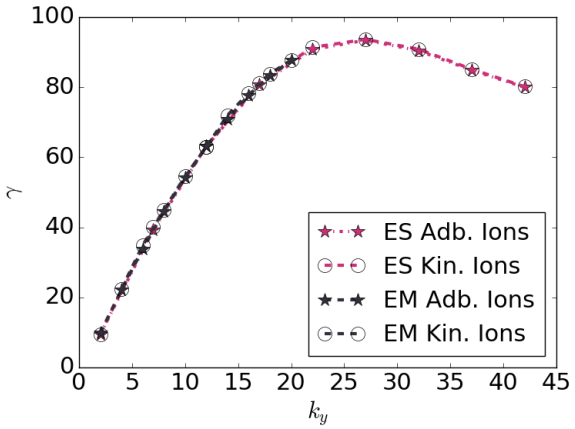

Figure 3.3: We see near-perfect match between electrostatic and electromagnetic linear runs in s-alpha geometry. This agreement shows that the ETG mode is independent of electromagnetic effects, allowing us to turn these off in a simulation. Turning off EM effects can drastically reduce computation time.

Given these results, we confirm that ETG modes in GENE are unaffected by

non-adiabatic ions and electromagnetic effects. While including these for linear runs does not greatly affect performance, performance of nonlinear GENE simulations will vastly improve by not including these parameters.

3.2 JET shot 78697

The input parameters for all JET runs are derived from data provided by JET. The data used the Hager bootstrap current model. Geometry for the simulations is generated via EFIT using the provided .eqdisk file provided. A number of input parameters, including Z_{eff}, were detected by GENE via the provided .iterdb file. Chosen normalized radii for analysis are $r = 0.95$, 0.96, 0.97, 0.98, from the top of the pedestal to the middle of the pedestal, respectively. The temperature vs radius plot of the pedestal from this shot is shown in Fig. 3.5, with selected radii shown.

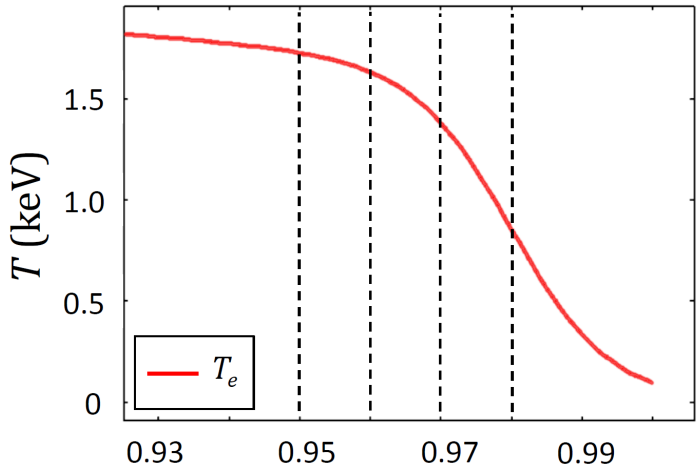

Figure 3.4: Shown is the last $\sim 7\%$ of the temperature profile, the region known as the pedestal, for JET shot 78697. At $r \approx 0.95$, the pedestal ends and at $r \approx 0.98$, we see the sharpest gradient.

3.2.1 Linear JET runs

A simple set of k_y scans are run for linear analysis. We scan over a range of k_y values typical of ETG modes. We see that for shallow temperature gradients, near the top of the pedestal, we have relatively low growth rates and for steep temperature gradients, near the middle of the pedestal, we have much higher growth rates, all as we assume should happen from linear ETG modes.

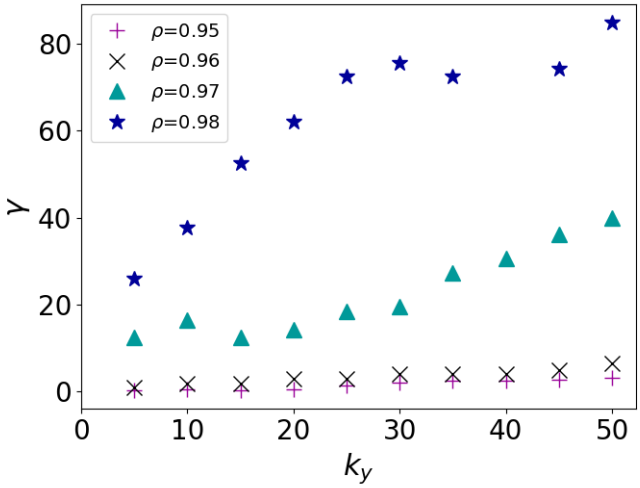

Figure 3.5: Plotted are linear growth rates, γ, for a range of k_y values, at the top ($\rho = 0.95$) to the middle ($\rho = 0.98$) of the pedestal. As expected, growth rates are high for the middle of the pedestal, i.e., the steepest temperature gradient, and low for the top of the pedestal, i.e., the shallowest temperature gradient.

3.2.2 Nonlinear JET runs

While linear simulations help to verify that our data is producing expected results for growth rate, we must use nonlinear simulations to truly delve into what is happening. We first look at heat flux produced by the ETG instability. Our analysis finds significant heat flux for ETG scale instabilities in the pedestal region, including at the top of the pedestal where there is a much shallower temperature gradient than in the middle of the pedestal.

Because the predominant driver of this instability is the electron-temperature gradient, a currently unknown mechanism is causing this unexpectedly high heat flux at the pedestal top for ETG instabilities. Plotting maps of the electrostatic field in our box, we find large streamers forming at the top of the pedestal, while none are found in the middle of the pedestal.

3.2.2.1 Nonlinear saturation

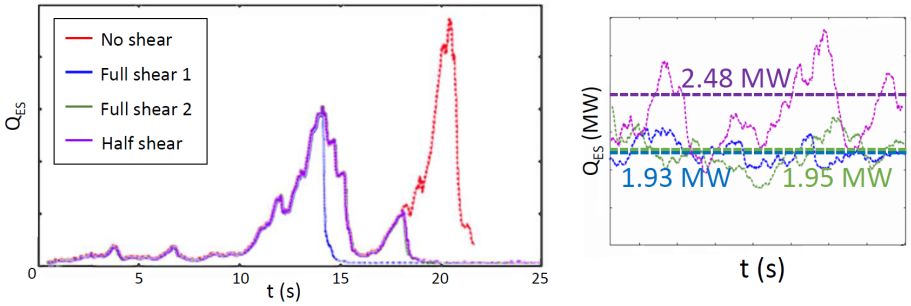

Figure 3.6: Left shows heat flux, in arbitrary units, for all four sets of nonlinear runs. The no (velocity) shear run never saturates. Full shear run #1 continues from checkpoint #4, saturating quickly. Full shear #2 and half shear runs continue from checkpoint #6, also saturating quickly. Right shows heat-flux saturation, at arbitrary times spanning 4 s of simulation time, of all three runs that saturated, full shear #1, full shear #2, and half shear, along with time-averaged heat flux in MW.

While GENE is solving the nonlinear equations, the calculated heat flux can fluctuate wildly until a statistical saturation is found. Saturation may not be achieved in a single simulation, so it is necessary to use GENE's checkpoint feature for nonlinear runs. The checkpoint file contains all information at the time that the simulation ends, so continuing from a checkpoint file allows us

to continue the calculations. For $r = 0.96, 0.97, 0.98$, saturation is achieved by the second run, shown in Fig. 3.6. However, for $r = 0.95$, corresponding to the top of the pedestal, we initially find no saturation after seven simulations. As available computer time is limited, we don't continue on. But, to check effects of velocity shear on heat flux, we take two separate checkpoints, #4 and #6, and continue from there with shear included, shown in Figure 3.6. From checkpoint #6, we include full shear, `ExBrate = -0.76`, and half shear, `ExBrate = -0.38`, in two separate sets of runs to check the dependence of shear on heat flux. From checkpoint #4, we include full shear, to test against the value found from continuing from checkpoint #6.

3.2.2.2 Heat flux

Heat flux found is shown in Table 3.1. We find heat flux for all sets of runs except at $r = 0.95$ with no shear included, as that set never saturated. However, we find non-negligible heat flux, ranging from 5.8%, at the top, to 8.2%, in the middle, of total input power, ~ 33 MW. Our lowest heat flux is seen at $r = 0.96$, a bit after the top of the pedestal, with only 1.7% of the total input power.

Comparing the highest heat flux at the pedestal top, 2.48 MW from including our half-shear value, to the heat flux at the pedestal middle, 2.71 MW, we see only 8.4% difference between the two. As ETG-driven instabilities are primarily driven by temperature gradient, which is `omt = 3.42` at the top and `omt = 69.48` at the middle, we see that there is

Radius [Shear value]	Heat flux (MW)
0.95 [Full shear 1]	1.93
0.95 [Full shear 2]	1.95
0.95 [Half shear]	2.48
0.95 [No shear]	-
0.96 [No shear]	0.59
0.97 [No shear]	1.39
0.98 [No shear]	2.71

Table 3.1: Heat flux values for each set of nonlinear simulations at varying radii.

a phenomenon beyond temperature gradient producing the heat flux from the ETG mode. And, as we see from our linear results, our linear growth rates are low at the top and high in the middle, we posit that this as-of-yet-unknown phenomenon is purely nonlinear in nature.

3.2.2.3 Streamer formation and velocity shear

A quick way to check for streamer formation is to look at maps of the electrostatic potential in GENE, shown in Figure 3.7. For $r = 0.96, 0.97, 0.98$, we find small structures, and thus no streamers, in the potential maps. However, for $r = 0.95$, we find large structures, i.e., streamers, throughout the simulations, until velocity shear is turned on. Once shear is turned on, the structures begin to break up, becoming small-scale structures by the end of each set of simulations.

Comparing the half-shear potential maps to the full-shear potential maps shows evidence of streamer dependence on shear. We see in Figure 3.7 that larger-scale structures are present in the half-shear potential than in both of

the full-shear potentials. We can thus infer that stronger shear results in smaller potential structures, thus further suppression of streamers and transport.

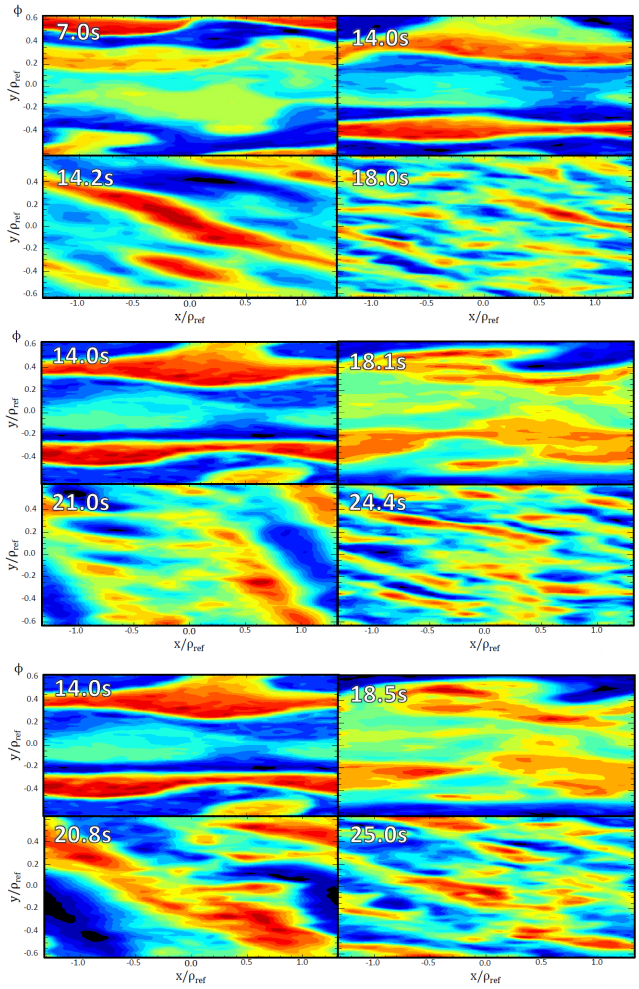

Figure 3.7: Electrostatic potential maps shown for full shear (FS) run #1 (top), FS run #2 (middle), and half shear (HS) run (bottom), with simulation times shown for each map. The first frame (top left) of each shows the potential well before the shear is turned on. The second frame (top right) of each shows the potential just after shear is turned on. The third (bottom left) frame shows the start of streamer dissipation. And, fourth (bottom right) frame shows the potential at the end of each simulation. Soon after turning on velocity shear, streamers start to break up for all cases. With the lower shear value, HS, we see larger structures at the end of the simulation–suggesting the level of velocity shear is a strong cause of streamer dissipation.

Chapter 4

Conclusion

In summary, this thesis has verified a number of questions concerning electron-temperature gradient modes in the pedestal, while bringing up more questions in the process. We have found that electromagnetic effects and kinetic ions do not influence linear ETG simulations for the cyclone case and s-alpha geometry. We also found a relationship between heat flux, streamers, and velocity shear in simulations run from experimental Joint European Torus data.

Regarding electromagnetic effects and kinetic ions on linear ETG simulations, our results were expected. We know that ETG turbulence is electrostatic in nature, thus the inclusion of electromagnetic effects should cause no change on a simulation. Additionally, given that ion oscillations are more than an order of magnitude larger than electron fluctuations, we expected to see no change in results when including kinetic ions. We observed both of these assumptions to hold true in linear simulations. While we stated that no nonlinear investigation of these effects, we can assume that the results hold for nonlinear simulations, as the nonlinear operator in GENE contains only terms mixing perpendicular wave modes.

With the analysis of JET shot 78697, we found non-negligible heat flux throughout the pedestal, upwards of 10% of the total output heat. While our linear analysis showed growth rates that follow the basic workings of the ETG mode, low growth rates at shallow temperature gradients and high growth rates at steep temperature gradients, the heat fluxes found did not fit this trend, thus begging the question: what else is contributing to the heat flux?

Working with the nonlinear simulations at the pedestal top, the heat flux did not saturate with our base input parameters, though the flux did saturate at all three radii further into the pedestal. This statistical saturation is necessary for meaningful results. In the interest of wisely using computation time, we stopped waiting for the unaltered data to saturate and moved onto simulations with induced velocity shear, though saturation may be found from subsequent simulations of the base. Using two separate checkpoints, we included velocity shear, finding that the flux quickly saturated within one subsequent run. At one checkpoint we tested two values of velocity shear, what we dubbed "full" and "half", and tested the "full" shear at the other checkpoint. We found agreement of heat flux between the two "full" shear results and saw higher heat flux from the "half" shear simulation. A possible explanation of these findings lies in streamer formation.

In our investigation, we found large streamers at the pedestal top, the shallow-gradient region, while no evidence of streamers were seen in the pedestal middle, the steep-gradient region. As streamers are large-scale structures that span across flux surfaces, greater than normal heat flux can

be seen when streamers are present. We find that the inclusion of velocity shear breaks apart streamers in all three sets of simulations that included shear. For the simulations that had "full" shear, we saw much smaller structures at the end of the simulations than we saw with the "half" shear simulation.

From these findings, we can infer a few things regarding ETG modes in the pedestal. One, streamer formation at the top of the pedestal causes a higher-than-expected heat flux for ETG modes. Two, velocity shear breaks apart streamers at this scale. Three, higher levels of velocity shear break apart streamers more effectively than lower levels of shear, lowering heat flux caused by ETG modes. Last, given that pedestal conditions typically cause high velocity shear, it is plausible that pushing high velocity shear deeper into the plasma will lead to an extended pedestal.

Future Work

As for results of EM effects and kinetic ions on nonlinear simulations, a nonlinear study could be undertaken to confirm these do not affect nonlinear simulations. Further, including in that study simulations using experimental data, such as the JET data used in this thesis, would be beneficial.

Regarding the pedestal analysis, a good deal of future work is necessary to further motivate these findings. For one, concerning JET shot 78697, extended analysis is important. A continued simulation to check for saturation at the pedestal top, given plenty of computation time, will tell us

what the ETG-driven heat flux at the pedestal top truly was for this shot. Additionally, this thesis looked at only the outboard midplane of this shot, thus extending analysis beyond that, looking at the top and bottom of the tokamak, as well as the inboard midplane, will explain what is happening elsewhere in the tokamak. Beyond analysis of this shot, repeating the analysis on more shots will be necessary to verify that these are not one-off findings. Namely, shots from DIIID, as well as more shots from JET, including ITER-like-wall shots, as shot 78697 was from a carbon-wall shot. Extending beyond these devices may prove useful, as well. Lastly, performing this analysis on internal transport barriers will help shed more light on conditions and control of transport barriers other than the pedestal.

Bibliography

[1] Richard Gerber at NERSC. Edison overview. 2013.

[2] S. I. Braginskii. Transport processes in a plasma. *Reviews of Plasma Physics 1*, page 205, 1965.

[3] FusionWiki by LNF and Fusenet. Ion temperature gradient instability, http://fusionwiki.ciemat.es/wiki/, 2016.

[4] M. A. Beer S. C. Cowley and G. W. Hammett. Fieldaligned coordinates for nonlinear simulations of tokamak turbulence. *Physics of Plasmas*, 2(2687), 1995.

[5] T. Görler T. Dannert F. Merz D. Told P. Xanthopoulos T. Bird X. Lapillonne S. Brunner GENE dev team and F. Jenko. Gyrokinetic turbulence investigations with gene - the numerics behind and some applications. Numerical Methods for the Kinetic Equations of Plasma, 2013.

[6] M. J. Bertin et al. *Pisot and Salem Numbers*. user Verlag, Berlin, 1992.

[7] GENE. Gyrokinetic electromagnetic numerical experiment, http://www.gkw.org.uk.

[8] GKW. Gkw a tool for fusion energy research, http://www.genecode.org.

[9] GS2. Itg: Cyclone base case, http://gs2.sourceforge.net/pmp/itg.html, 2004.

[10] R. D. Hazeltine and J. D. Meiss. *Plasma Confinement*. Dover, 2003.

[11] S. C. Cowley W. Dorland I. G. Abel G. G. Plunk E. Wang M. Barnes and A. A. Schekochihin. Multiscale gyrokinetics for rotating tokamak plasmas: fluctuations, transport and energy flows. *Reports on Progress in Physics*, 76, 2013.

[12] Donald K. Knuth. *The TEXbook*. Addison-Wesley, 1984.

[13] W. Dorland F. Jenko M. Kotschenreuther and B.N. Rogers. Electron temperature gradient turbulence. *Physical Review Letters*, 85(26), December 2000.

[14] Leslie Lamport. *LATEX: A document preparation system*. Addison-Wesley, 2nd edition, 1994.

[15] A. W. Leonard. Edge-localized-modes in tokamaks. *Physics of Plasmas*, 21, 2014.

[16] F. Mittelbach M. Goosens and A. Samarin. *The LATEXCompanion*. Addison-Wesley, 1994.

[17] F. Merz. *Gyrokinetic Simulation of Multimode Plasma Turbulence*. PhD thesis, Westf"alischen Wilhelms-Universität M"unster, 2009.

[18] W. L. Rowan C. C. Klepper C. P. Ritz R. D. Bengtson K. W. Gentle P. E. Phillips T. L. Rhodes B. Richards and A. J. Wootton. Global

particle confinement in the texas experimental tokamak. *Nuclear Fusion*, 27, 1987.

[19] Michael Spivak. *The joy of TEX*. American Mathematical Society, Providence, R.I., 2nd edition, 1990.

[20] W. M. Stacey. *Fusion Plasma Physics*. Wiley-VCH, 2nd edition, 2012.

[21] D. Told. *Gyrokinetic Microturbulence in Transport Barriers*. PhD thesis, Universität Ulm, 2012.

[22] Alf J. van der Poorten. Some problems of recurrent interest. Technical Report 81-0037, School of Mathematics and Physics, Macquarie University, North Ryde, Australia 2113, August 1981.

Vita

Austin Lee Blackmon was born in York, Nebraska in 1988 to Bryan and Cecelia Blackmon. She received the Bachelor of Science degree in Physics from the University of Illinois at Urbana-Champaign in 2015. She entered the PhD program in Physics at the University of Texas at Austin the same year. Finding herself more interested in programming and data analysis and less interested in the physics of her graduate work, she decided to opt out of the doctorate program, instead finishing with a Master of Arts in Physics in 2019.

Permanent contact: austin@blackmountains.space

This thesis was typeset with LaTeX[†] by the author.

[†]LaTeX is a document preparation system developed by Leslie Lamport as a special version of Donald Knuth's TeX Program.